Monthly Notices of the ROYAL ASTRONOMICAL SOCIETY

MNRAS **507,** 466–474 (2021) https://doi.org/10.1093/mnras/stab2166
Advance Access publication 2021 July 30

Chemical abundances in Seyfert galaxies – VI. Empirical abundance calibration

Oli L. Dors ★

Universidade do Vale do Paraíba, Instituto de Pesquisa & Desenvolvimento, Avenida Shishima Hifumi, 2911, Cep 12244-000, São José dos Campos, SP, Brazil

Accepted 2021 July 22. Received 2021 July 21; in original form 2021 April 4

ABSTRACT

We derived a bi-dimensional calibration between the emission-line ratios $R_{23} = ([\mathrm{O\,II}]\,\lambda3726 + \lambda3729 + [\mathrm{O\,III}]\,\lambda4959 + \lambda5007)/\mathrm{H}\,\beta$, $P = [([\mathrm{O\,III}]\,\lambda4959 + \lambda5007)/\mathrm{H}\,\beta]/R_{23}$ and the oxygen abundance relative to hydrogen (O/H) in the gas phase of Seyfert 1 and 2 nuclei. In view of this, emission-line intensity ratios for a sample of objects taken from the Sloan Digital Sky Survey Data Release 7 measured by the MPA/JHU group and direct estimates of O/H based on T_e-method, adapted for active galactic nuclei (AGNs), are considered. We find no variation of R_{23} observed along the radii of AGNs, which shows that this line ratio is a good oxygen abundance (O/H) indicator for the class of objects considered in this work. The derived O/H $= f(R_{23}, P)$ relation produces O/H values similar to estimations via T_e-method in a wide range of metallicities [$8.0 \lesssim 12 + \log(\mathrm{O/H}) \lesssim 9.2$]. Conversely to star-forming regions in the high-metallicity regime, R_{23} shows a positive correlation trend with O/H in AGNs. This indicates that the hardness of ionizing radiation is not affected by the metallicities in these objects or narrow-line regions are not significantly modified by changes in the spectral energy distribution due to metallicity variations.

Key words: ISM: abundances – galaxies: abundances – galaxies: active – galaxies: evolution – galaxies: nuclei – galaxies: Seyfert.

1 INTRODUCTION

Active galactic nuclei (AGNs) and star-forming regions (SFs) present in their spectra strong metal and hydrogen emission lines, whose relative intensities can be used to derive the metallicity and/or the abundances of heavy elements. These features make these objects essential for studying the chemical evolution of galaxies.

It is widely known that the most dependable approach for determining the chemical abundance of heavy elements (e.g. O, N, and S) in the gas phase of SFs and planetary nebulae is primarily based on direct measurements of the electron temperature (T_e), which is commonly referred to as the T_e-method (for a review, see Peimbert, Peimbert & Delgado-Inglada 2017; Pérez-Montero 2017; Maiolino & Mannucci 2019). Basically, this method consists of determining the T_e of the gas phase through emission-line intensity ratios emitted by a given ion and originated in transitions from two levels with considerably different excitation energies. For example, the T_e for the gas regions where the O^+, O^{2+}, and N^+ ions are located can be determined through the $[\mathrm{O\,II}](\lambda3726 + \lambda3729)/(\lambda7319 + \lambda7330)$, $[\mathrm{O\,III}](\lambda4959 + \lambda5007)/\lambda4363$, and $[\mathrm{N\,II}](\lambda6548 + \lambda6584)/(\lambda5755)$ line ratios, respectively (e.g. Hägele et al. 2008). However, for most extragalactic objects where the T_e-method can be applied, which has only the $[\mathrm{O\,III}](\lambda4959 + \lambda5007)/\lambda4363$ line ratio measured, it is only possible to estimate the temperature for the high-ionization zone (e.g. van Zee et al. 1998). In these cases, temperatures for the low-ionization zones are obtained from empirical (e.g. Kennicutt Robert, Bresolin & Garnett 2003; Pilyugin, Vílchez & Thuan 2006; Pilyugin 2007; Esteban et al. 2009; Berg et al. 2015; Croxall et al. 2016; Yates et al. 2020) or photoionization model (e.g. Campbell, Terlevich & Melnick 1986; Garnett 1992; Pagel et al. 1992; Izotov, Thuan & Lipovetsky 1997; Deharveng et al. 2000; Pérez-Montero & Contini 2009; Pérez-Montero 2014) relations, which can introduce some uncertainty in the abundance determinations (e.g. Arellano-Córdova & Rodríguez 2020).

The reliability of the T_e-method is supported by the agreement between oxygen abundance relative to hydrogen (O/H) estimates in H II regions located in the solar neighbourhood and those derived through the weak interstellar O I $\lambda1356$ Å line towards the stars (see Pilyugin 2003, and references therein). Moreover, a consonance has been found between oxygen abundances obtained for SFs and B-type stars in the Milky Way and other nearby galaxies (see Toribio San Cipriano et al. 2017, and references therein). However, the determination of T_e requires measurements of auroral emission lines (e.g. $[\mathrm{O\,III}]\lambda4363$ Å, $[\mathrm{N\,II}]\lambda5755$ Å, and $[\mathrm{S\,III}]\lambda6312$ Å), which are generally weak (about 100 times weaker than H β) in the spectrum of objects with high metallicity and/or low excitation (e.g. van Zee et al. 1998; Díaz et al. 2007; Dors et al. 2008). To circumvent this limitation of the T_e-method, Pagel et al. (1979), following the original idea of Jensen, Strom & Strom (1976), proposed the use of the $R_{23} = ([\mathrm{O\,II}]\lambda3726 + \lambda3729 + [\mathrm{O\,III}]\lambda4959 + \lambda5007)/\mathrm{H}\,\beta$ line ratio as O/H abundance indicator for SFs. After the aforementioned pioneering work, several authors have proposed calibrations for SFs between R_{23} and the O/H abundance as well as considerations for other line ratios (for a review, see Lopez-Sanchez & Esteban 2010). Basically, there are two ways to obtain a calibration between strong emission-line ratios and O/H (a metallicity tracer), i.e. assuming predictions from photoionization models (e.g. McGaugh 1991; Kewley & Dopita 2002) and by using observational emission lines and O/H abundance values derived from the T_e-method (e.g. Storchi-

* E-mail: olidors@univap.br

Bergmann, Calzetti & Kinney 1994; Pilyugin 2000, 2001; Yin et al. 2007; Marino et al. 2013; Jiang et al. 2019). This method of utilizing calibration to estimate elemental abundances is known as strong-line method. It has been established that, for SFs, the majority of the strong-line methods based on theoretical models overestimate the O/H abundance as compared to the results obtained from the T_e-method (e.g. Yin et al. 2007), where the discrepancies are of the order of 0.2–0.3 dex (Lopez-Sanchez & Esteban 2010).

In comparison with SFs, there are few abundance estimates for AGNs derived from the T_e-method in the literature. In fact, it appears that most complete abundance determinations in AGNs based on the T_e-method were carried out by Osterbrock & Miller (1975), who derived the He, O, N, Ne, and Fe abundances, in relation to the hydrogen, in the gas phase of 3C 405 (Cygnus A). The majority of the other studies (e.g. Izotov & Thuan 2008; Dors et al. 2015, 2020b) have been focused on determining only the O/H abundance and a few for the N/H (e.g. Flury & Moran 2020). Furthermore, for the strong-line method based on narrow optical lines of AGNs, there are only theoretical calibrations proposed by Storchi-Bergmann et al. (1998) as well as semi-empirical calibrations proposed by Castro et al. (2017), Carvalho et al. (2020), and Dors et al. (2021). These calibrations are primarily based on photoionization models, which may have some uncertainties. First, the foregoing AGN calibrations consider lines emitted by oxygen and nitrogen, so it is important to assume a correct relation between O and N in the models (Pérez-Montero & Contini 2009). However, the N/H abundance is barely known in AGNs. In fact, Dors et al. (2017b), who used detailed photoionization models to reproduce narrow optical [$3000 < \lambda(\text{Å}) < 7000$] emission lines of a sample of AGNs, presented the first quantitative nitrogen abundance determination for a small sample of 44 Seyfert 2 nuclei in the local universe ($z \lesssim 0.1$; see also Hamann et al. 2002; Contini 2017; Pérez-Montero et al. 2019; Flury & Moran 2020). Secondly, photoionization models are subject to intrinsic uncertainties, e.g. all relevant physical processes are not treated correctly, inaccurate atomic data use, spherical geometry consideration, etc. (see Netzer & Ferland 1984; Viegas 2002; Kennicutt et al. 2003).

Recently, Dors et al. (2020b) investigated the discrepancy between O/H abundance estimations for narrow-line regions (NLRs) of Seyfert 2 derived by using T_e-method and those derived from photoionization models. These authors found that the derived discrepancies are mainly due to the inappropriate use of the relations between temperatures of the low (t_2)- and high (t_3)-ionization gas zones derived for H II regions in AGN chemical abundance studies. In addition, Dors et al. (2020b), using a photoionization model grid, derived a new expression for the t_2–t_3 relation valid for Seyfert 2 nuclei that reduces the O/H discrepancies between the abundances obtained from strong-line methods and those derived from T_e-method by ∼0.4 dex. This new methodology, combined with the very large sample of spectroscopic data made available by the Sloan Digital Sky Survey (SDSS; York et al. 2000), will help us to build an empirical calibration for AGNs, which is not available in the literature reviewed thus far.

Following from above, the emission-line intensities of the SDSS Data Release 7 (DR7; Abazajian et al. 2009) measured by the MPA–JHU group[1] and the methodology proposed by Dors et al. (2020b) are used in this study to calculate the O/H abundance for a sample of Seyfert 1 and 2 nuclei. Thereafter, following the methodology considered by Pilyugin (2000, 2001) and the same supposition for SFs – the strong oxygen lines [O II]λλ3726, 3729 Å and [O III]λλ4959, 5007 Å contain the necessary information required to accurately derive the O/H abundance (McGaugh 1991) – we obtain a bi-dimensional empirical calibration between the R_{23} and $P = ([\text{O III}]\lambda4959 + \lambda5007/\text{H}\,\beta)/R_{23}$ line ratios and O/H abundance, valid for AGNs. This study is organized as follows: In Section 2, the observational data and the methodology used to estimate the oxygen abundance are presented. The resulting calibration and the discussion are presented in Sections 3 and 4, respectively. Finally, the conclusion of the outcome is given in Section 5.

2 METHODOLOGY

To obtain a calibration between strong oxygen emission lines and the O/H abundance for AGNs, we selected from the SDSS DR7 spectroscopic data of confirmed sample of type 1 and 2 Seyfert nuclei. These data were used to calculate the O/H abundance through the T_e-method and, afterwards, an empirical calibration was derived. In what follows, each one of the procedures mentioned earlier is described.

2.1 Observational data

We used optical emission-line intensities of Seyfert 1 and 2 nuclei taken from the SDSS (Abazajian et al. 2009) DR7 and presented in Dors et al. (2020a) (hereafter Paper I). From these data, we considered only the intensities (in relation to H β) of the emission lines [O II]λ3726 Å + λ3729 Å, [O III]λ4363 Å, [O III]λ5007 Å, H α, [N II]λ6584 Å, [S II]λ6716 Å, and [S II]λ6731 Å. The lines measurements were carried out by the MPA/JHU group and they are reddening corrected (see Paper I).

The Seyfert 1 and 2 classifications were obtained by cross-correlation between the identification of each object in the SDSS data and in a catalogue provided by NED/IPAC[2] (NASA/IPAC Extragalactic Database). Here, we only considered objects for which the [O III]λ4363 Å line has a measurement error of less than 50 per cent of its intensity. Thereafter, to minimize the contribution of SF emission to the observed AGN fluxes, we only considered objects that are more than 0.1 dex (see Kewley et al. 2006) above the demarcation lines proposed by Kewley et al. (2001) to separate AGNs from SFs, where objects with

$$\log([\text{O III}]\lambda5007/\text{H}\,\beta) > \frac{0.61}{\log([\text{N II}]\lambda6584/\text{H}\,\alpha) - 0.47} + 1.19 \quad (1)$$

and

$$\log([\text{O III}]\lambda5007/\text{H}\,\beta) > \frac{0.61}{\log([\text{S II}]\lambda6725/\text{H}\,\alpha) - 0.32} + 1.30 \quad (2)$$

are classified as AGNs. The [S II]λ6725 Å line represents the sum of the [S II]λ6717 Å and [S II]λ6731 Å lines. This procedure resulted in a sample of 91 objects (35 Sy2 and 56 Sy1) with redshifts $z \lesssim 0.4$. The reader is referred to Paper I for a complete description about the observational data and aperture effects on metallicity/abundance estimation.

In contrast to previous studies (Carvalho et al. 2020; Dors et al. 2020a, b, 2021), Seyfert 1 nuclei are considered in this work. According to the unification scheme, the continuum source and the broad-line region are blocked by a dusty torus in Seyfert 2 (Antonucci 1993). However, it is not clear whether the torus effects extend to NLRs. For instance, Schmitt (1998), who compared optical emission-line intensities of distinct Seyfert classes, found that Seyfert 1

[1]Max Planck Institute for Astrophysics and John Hopkins University.

[2]ned.ipac.caltech.edu.

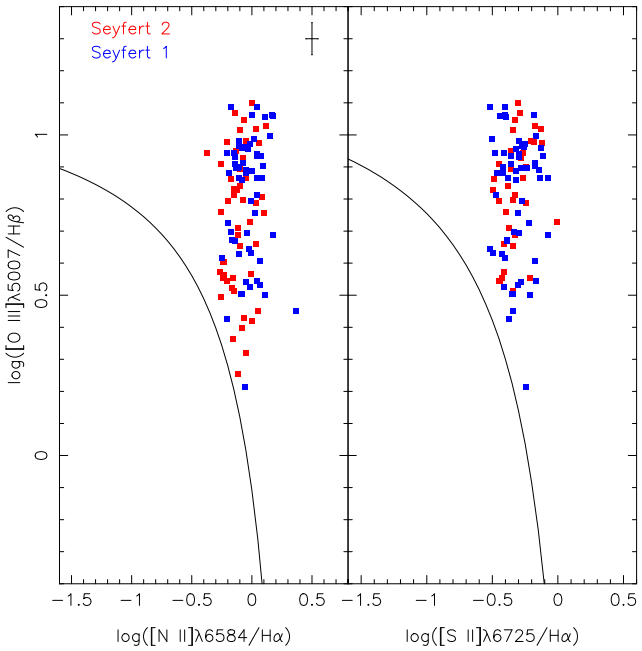

Figure 1. Diagnostic diagrams log ([O III]λ5007/H β) versus log[N II]λ6584/H α and versus log ([S II]λ6725/H α). Points represent objects of our sample (see Section 2.1), where objects classified as Seyfert 1 and 2 are represented by different colours, as indicated. Black lines, taken from Kewley et al. (2001) and represented by equations (1) and (2), separate objects ionized by massive stars from those ionized by AGN-like mechanism. Error bar, in the left-hand panel, represents the typical uncertainty (0.1 dex) in AGN emission-line ratio measurements (e.g. Kraemer et al. 1994).

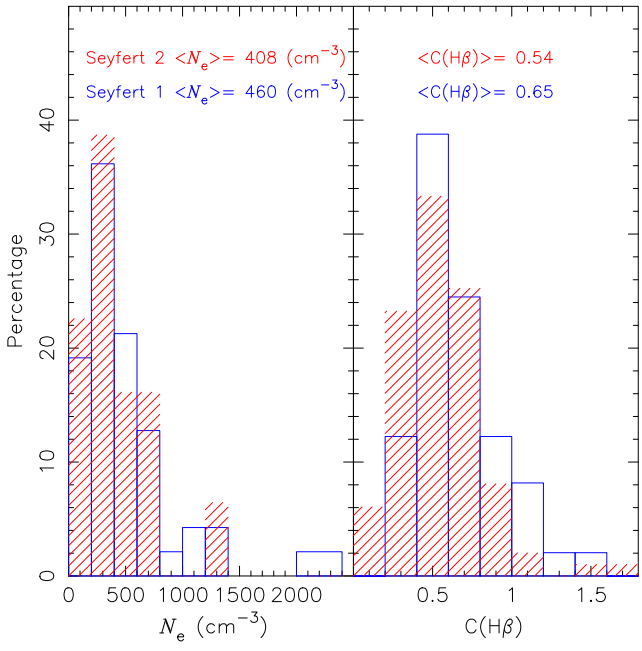

Figure 2. Histogram containing the distributions of electron density N_e (left-hand panel) and reddening correction C(H β) (right-hand panel) for our sample of objects (see Section 2.1). N_e is calculated through the emission-line ratio [S II]λ6717/[S II]λ6731.

nuclei have a higher excitation than Seyfert 2 nuclei. Zhang et al. (2008) used spectroscopic data of AGNs ($z < 0.3$) from the SDSS DR4 (Blanton et al. 2017) and found that Seyferts 1 and 2 have different distributions in the BPT (Baldwin, Phillips & Terlevich 1981) [O III]λ5007/H β versus [N II]λ6584/H α diagram. If Seyferts 1 and 2 of our sample show this difference in diagnostic diagrams, some potential biases could be introduced in the calibrations based on emission-line intensities from both kinds of AGNs. In order to verify this, the diagnostic diagrams [O III]λ5007/H β (ordinate) versus [N II]λ6584/H α (abscissa) and [S II](λ6716 + λ6731)/H α (abscissa) containing our sample of objects as well as the criteria to separate SFs from AGNs proposed by Kewley et al. (2001), i.e. equations (1) and (2), are shown in Fig. 1. In this figure, the line ratios of Seyferts 1 and 2 are indicated by different colours. It can be seen in Fig. 1 that Seyferts 1 and 2 occupy the same regions in both diagrams. Since the position of an object in diagnostic diagrams is driven by some physical parameters of the gas phase (e.g. Feltre, Charlot & Gutkin 2016), probably, these objects have similar ionization degree and metallicity. This result is apparently in disagreement with the findings obtained by Zhang et al. (2008); however, it is worthwhile to note that these authors considered a sample of objects with wider range of ionization, while we selected only objects that have the [O III]λ4363 Å line measured, i.e. objects with high excitation degree (see also Flury & Moran 2020).

Another concern in our analysis is about the electron density (N_e) of Seyfert 1, because the gas phase in this object class can reach high N_e values and some lines emitted by transitions between levels with low critical density N_c, such as [O II]λλ3726, 3729 Å ($N_c = 10^{3.7}$ cm^{-3}; Vaona et al. 2012), can suffer collisional de-excitation, resulting in incorrect abundance estimates. To verify the range of electron density of our sample, the N_e value for each object was derived through the relation between this parameter with the [S II]λ6717/[S II]λ6731 line ratio by using the iraf code (Tody 1986; De Robertis, Dufour & Hunt 1987; Shaw & Dufour 1995) and assuming an electron temperature value of 10 000 K. In Fig. 2, left-hand panel, the N_e distribution and the average value for our sample of Seyferts 1 and 2 are shown. It can be seen that both Seyfert types present similar distributions and average values of N_e. The maximum N_e value (2250 cm^{-3}), derived for a Seyfert 1 object, is a factor of ∼2 lower than the lowest critical density of the lines considered in the present analysis. Also in Fig. 2, right-hand panel, the reddening correction C(H β) distributions and the average values of these for our sample of objects are shown. We notice very similar distributions and average values for both Seyferts 1 and 2. From the analysis above, one can assume that the emission lines considered in this work are emitted in the gas phase of Seyferts 1 and 2 with similar physical conditions.

Typical uncertainty in AGN emission-line measurements considered in the present analysis is of the order of 0.1 dex (e.g. Kraemer et al. 1994).

2.2 O/H derivation

To calculate the abundance of oxygen in relation to hydrogen (O/H) through the T_e-method, we follow the same methodology developed by Dors et al. (2020b) for AGNs. This method is an adaptation of the T_e-method for H II regions but differing only in the t_2–t_3 assumed relation. Thus, it is hereafter referred to as T_e-method (AGN).

First, using the observational data for each object, the temperature for the high [t_3(obs.)]-ionization gas zone, i.e. for the nebular region where O^{2+} and ions with similar ionization potentials (e.g. Ne^{2+} and S^{2+}) are located, is derived from the expression

$$t_3(\text{obs.}) = 0.8254 - 0.000\,2415 \times R_{O3} + \frac{47.77}{R_{O3}}, \quad (3)$$

where $R_{O3} = [O\,III](\lambda4959\,Å + \lambda5007\,Å)/\lambda4363\,Å$ and t_3(obs.) is in units of 10^4 K. The t_3(obs.)–R_{O3} relation depends on the atomic data used to derive the emissivities of the emission lines involved and it suffers some uncertainties. In fact, different t_3(obs.)–R_{O3} relations have been proposed by several authors along the years (e.g. Pagel et al. 1992; Izotov et al. 2006; Hägele et al. 2008; Pérez-Montero 2014) and different temperature values of the order of some hundreds, for a given R_{O3} value, have been derived when distinct relations are considered. Equation (3) is valid for the range $30 \lesssim R_{O3} \lesssim 700$ with a corresponding temperature range of $0.70 \lesssim t_3(\text{obs.}) \lesssim 2.3$. In this study, only objects with t_3(obs.) in this range of values were considered.

Since it is not possible to estimate the temperature for the low [t_2(obs.])-ionization gas zone, i.e. for the nebular region where O^+ and ions with similar ionization potentials (e.g. S^+ and N^+) are located, due to the absence of the [N II]λ5755 and [O II]λλ7319, 7330 observational line intensities, the following theoretical relation between t_2 and t_3 has been adopted:

$$t_2 = \left(a \times t_3^3\right) + \left(b \times t_3^2\right) + (c \times t_3) + d, \quad (4)$$

where $a = 0.17$, $b = -1.07$, $c = 2.07$, and $d = -0.33$ and t_2 is in units of 10^4 K. This t_2–t_3 relation was derived by Dors et al. (2020b) based on the photoionization model results built by Carvalho et al. (2020). This grid of models takes into account a wide range of nebular parameters, which are summarized below:

(i) Spectral energy distribution (SED): It is made up of two parts that are added together. The first is a Big Bump component that peaks at ≈1 Ryd and is parametrized by the temperature of the bump, which is assumed to be 5×10^5 K. The second component is an X-ray power law with a spectral index $\alpha_x = -1$ that is only added for energies greater than 0.1 Ryd to prevent it from extending into the infrared region. The α_{ox} spectral index defined as the slope of a power law between 2 keV and 2500 Å was assumed to vary from −0.8 to −1.4 (see Krabbe et al. 2021, for a detailed description of this SED).

(ii) Metallicity: Values for the metallicity in relation to the solar ($Z/Z_\odot$) = 0.2, 0.5, 0.75, 1.0, 1.5, and 2.0 were assumed in the models. All the abundances for the heavy metals were linearly scaled with the solar abundance[3] with the exception of nitrogen where we adopted the relation $\log(N/O) = 1.29 \times [12 + \log(O/H)] - 11.84$.

(iii) Electron density (N_e): The N_e was considered to be constant along the radius of AGN and the values 100, 500, and 3000 cm^{-3} were assumed.

(iv) Ionization parameter: The range of the logarithm of the ionization parameter was considered to be $-4.0 \leqq \log U \leqq -0.5$, with a step of 0.5 dex.

The t_2 and t_3 values predicted by the models correspond to the mean temperature for O^+ and O^{2+} over the nebular AGN radius times the electron density. Therefore, the t_2(obs.) and t_3(obs.) temperatures, calculated through integrated measurements of the flux of observational emission lines, could differ from those predicted by the models. In Riffel et al. (2021), the relation t_2–t_3 (equation 4) was compared with direct estimations of electron temperatures, calculated from observational auroral emission lines, for a small sample of AGNs (11 objects) and a good agreement was found between them. However, these authors showed that when outflowing gas is present in AGNs, a large deviation of direct electron temperature values from those derived through equation (4) is obtained.

Additionally, the O^{2+}/H^+ and O^+/H^+ ionic abundances were estimated using the following relations:

$$12 + \log\left(\frac{O^{2+}}{H^+}\right) = \log\left(\frac{1.33 \times I(5007)}{I(H\,\beta)}\right) + 6.144 + \frac{1.251}{t_3(\text{obs.})} - 0.55 \log t_3(\text{obs.}) \quad (5)$$

and

$$12 + \log\left(\frac{O^{+}}{H^+}\right) = \log\left(\frac{I(3727)}{I(H\,\beta)}\right) + 5.992 + \frac{1.583}{t_2} - 0.681 \log t_2 + \log(1 + 2.3 n_e), \quad (6)$$

where n_e is the electron density N_e in units of 10 000 cm^{-3}. For each object, the value of t_3(obs.) is obtained by using equation (3). The value of t_2 is derived by applying t_3(obs.) in the theoretical relation represented by equation (4). The same procedure is usually carried out in H II region abundance studies in scenarios where t_2(obs.) cannot be derived (e.g. Garnett 1992; Kennicutt et al. 2003.)

Finally, the total oxygen abundance (O/H) was derived assuming

$$\frac{O}{H} = \text{ICF(O)} \times \left[\frac{O^{2+}}{H^+} + \frac{O^+}{H^+}\right], \quad (7)$$

where ICF(O) is the ionization correction factor for oxygen that takes into account the contribution of unobserved oxygen ions (e.g. O^{3+}). To derive ICF(O), it is necessary to have the He^+/H^+ and He^{2+}/H^+ abundances (e.g. Torres-Peimbert & Peimbert 1977; Izotov et al. 2006), which it is not possible to derive because the helium recombination line λ4686 Å is not available in our data sample. Therefore, we assume for all objects an average value of 1.20 for ICF(O), which translates into an abundance correction of 0.1 dex, i.e. in order of the uncertainty derived in T_e-method estimates (e.g. Kennicutt et al. 2003; Hägele et al. 2008). This value represents the average for the values derived by Dors et al. (2020a), who found ICF(O) values ranging from 1.00 to 1.80 for a sample of local Seyfert 2.

We assume the typical uncertainty in the O/H estimates to be of the order of 0.1 dex, as estimated in Flury & Moran (2020).

3 O/H CALIBRATION

To calibrate a certain line ratio with the abundance, initially, it is necessary to analyse if the line ratio being considered has a secondary dependence on other physical parameters, usually, on the ionization degree of the gas. In the case of the R_{23} line ratio, McGaugh (1991) suggested that its use as O/H indicator for SFs must be conciliated with the O32 = ([O III]λ4959 + λ5007)/[O II]λ3727, where [O II]λ3727 is the sum of λ3726 and λ3729. The O32 line ratio has a strong dependence on the ionization degree of the gas and/or on the effective temperature of the hottest ionizing stars of SFs (see Pilyugin 2001; Dors & Copetti 2003; Dors et al. 2017a). Thus, any R_{23} calibration would consider line ratios dependent on the hardness of the ionizing radiation (Pilyugin 2001).

In relation to the R_{23} application as O/H abundance indicator for AGNs, Dors et al. (2015), by using results of a grid of photoionization models, showed that the R_{23}–O/H relation is dependent on the number of ionizing photos Q(H) or on the ionization parameter (U) of the gas [$U \propto Q$(H)]. Following Pilyugin (2001), we adopt the line ratio

[3]The solar composition assumed in the CLOUDY code is listed in http://web.physics.ucsb.edu/phys233/w2014/hazy1_c13.pdf.

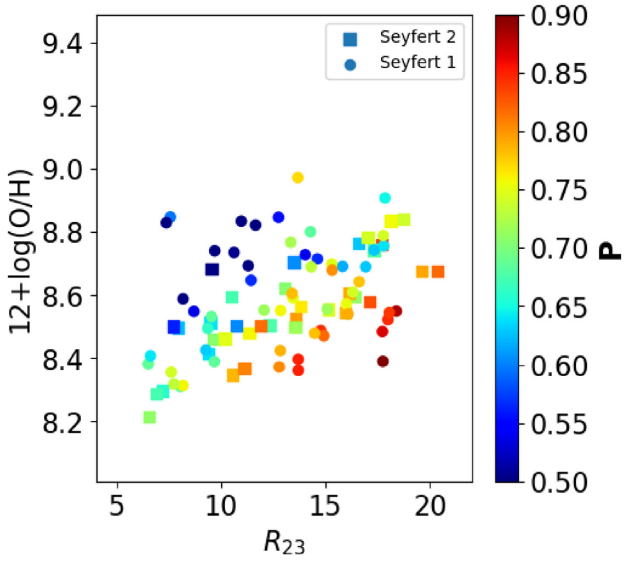

Figure 3. Oxygen abundance [in units of 12 + log (O/H)] versus R_{23} for our sample of objects (see Section 2.1). O/H abundances are calculated by using the T_e-method (AGN). Seyfert 1 and 2 nuclei are represented by different symbols and colour bars indicate the P value for each object.

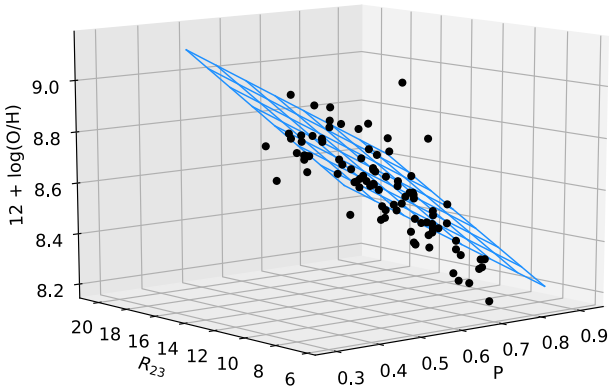

Figure 4. Bi-dimensional calibration between the oxygen abundance [in units of 12 + log (O/H)], $R_{23} = ([O\,II]\lambda3726 + \lambda3729 + [O\,III]\lambda4959 + \lambda5007)/H\,\beta$ and $P = ([O\,III]\lambda4959 + \lambda5007/H\,\beta)/R_{23}$. The surface represents the fit to the points given by equation (9). Points represent the line ratio intensities of our sample of objects (see Section 2.1) with the corresponding O/H abundance obtained by using the T_e-method (AGN) (see Section 2.2).

defined as

$$P = [([O\,III]\lambda4959 + \lambda5007)/H\,\beta]/R_{23} \quad (8)$$

as an indicator of the hardness of the ionizing radiation. In order to verify the dependence of R_{23} on the hardness of the ionizing radiation by using our data, in Fig. 3, the oxygen abundance derived through the T_e-method (AGN) for each object of our data sample versus the corresponding R_{23} value is shown. In this figure, the colour bars indicate objects with different P values while objects classified as Seyferts 1 and 2 are represented by different symbols. We notice the following:

(i) Seyferts 1 and 2 show similar O/H abundances and P values, and

(ii) the O/H–R_{23} relation for AGNs is dependent on P; hence objects with lower P values are located at the top-left region in Fig. 3.

The fact that O/H–R_{23} relation is dependent on P indicates that a bi-parametric calibration O/H = $f(R_{23}, P)$ is more accurate for AGNs instead of O/H = $f(R_{23})$. In view of this, the R_{23}, P, and 12 + log (O/H) values are shown in Fig. 4. A fit to the points, by using the least-squares method, results in the following expression:

$$Z = (-1.00 \pm 0.09)P + (0.036 \pm 0.003)R_{23} + (8.80 \pm 0.06), \quad (9)$$

where $Z \equiv 12 + \log(O/H)$. We refer to this approach as the D-method.

4 DISCUSSION

The estimation of O/H abundance through strong emission lines was first proposed by Jensen et al. (1976). Based on the behaviour of the intensity of optical emission-line ratios across the disc of some nearby spiral galaxies, mainly caused by radial abundance gradients as originally proposed by Searle (1971), Jensen et al. (1976) suggested that the [O III]λ5007/H β and [N II]λ6584/[O II]λ3727 line ratios can be chemical enrichment indicators. Between these two line ratios, these authors posited that [O III]/H β shows some advantages over [N II]/[O II]; however, any calibration between these line ratios and O/H can be obtained. Thereafter, Pagel et al. (1979) introduced the R_{23} line ratio as an O/H abundance indicator. These authors, by using O/H estimates based on T_e-method for the disc of H II regions and predictions from theoretical models built by Sarazin (1976), Shields & Searle (1978), and Stasińska (1978), proposed the first calibration between strong line ratios and O/H abundance for SFs (for other pioneering papers, see, for instance, Alloin et al. 1979; Stasińska et al. 1981; Shaver et al. 1983; Edmunds & Pagel 1984). The first empirical calibration between strong emission lines and O/H abundances derived through the T_e-method seems to have been proposed by Storchi-Bergmann et al. (1994),[4] who presented an SF calibration using the N2 = ([N II]λ6548 + λ6584)/H α line ratio as an abundance indicator (see also Pettini & Pagel 2004; Liang et al. 2007; Shi, Zhao & Liang 2007; Yin et al. 2007; Pilyugin, Grebel & Mattsson 2012; Marino et al. 2013; Morales-Luis et al. 2014; Jones, Martin & Cooper 2015; Brown, Martini & Andrews 2016; Pilyugin & Grebel 2016; Sanders et al. 2016; Bian, Kewley & Dopita 2018; Gburek et al. 2019; Jiang et al. 2019).

In regard to AGNs, the first strong emission line calibrations were proposed by Storchi-Bergmann et al. (1998), who by using photoionization model results proposed two bi-dimensional calibrations among N2–[O III]/H β, N2–[O II]/[O III] narrow-line ratios and O/H abundance. Thereafter, theoretical (e.g. Dors et al. 2014, 2015) and semi-empirical (e.g. Castro et al. 2017; Carvalho et al. 2020; Dors et al. 2021) calibrations as well as Bayesian-like approach to derive AGN chemical abundances (e.g. Thomas et al. 2018; Mignoli et al. 2019; Pérez-Montero et al. 2019) have been proposed. Recently, Flury & Moran (2020) developed an approach for estimating abundances of heavy elements, which involves a reverse engineering of the T_e-method and considering the [O III]λ5007/H β versus [N II]λ6584/H α diagnostic diagram. This methodology, which is only based on strong emission lines, consistently recovers O/H and N/H abundance values calculated through the T_e-method with an uncertainty of about 0.2 dex. The method proposed by Flury &

[4]For a review on empirical calibration for SFs and their limitations, see Kewley, Nicholls & Sutherland (2019).

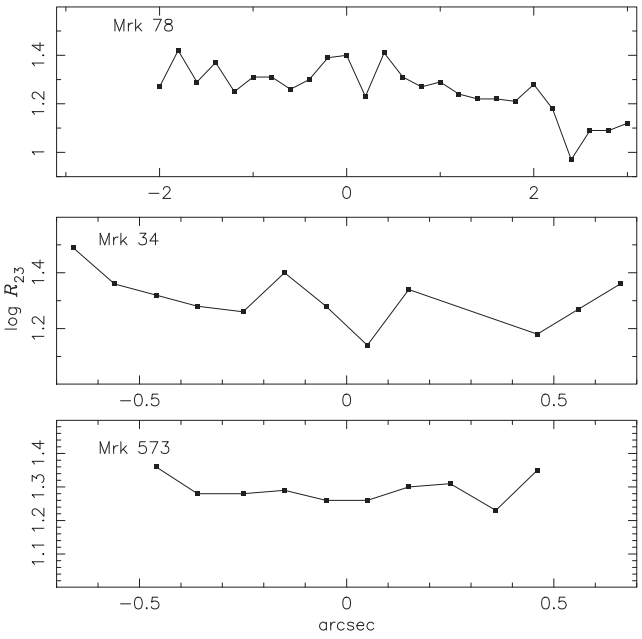

Figure 5. Logarithm of R_{23} as a function of distance (in arcsec) from the centre of three AGNs, as indicated. The data for Mrk 573, Mrk 34, and Mrk 78 were taken from Revalski et al. (2018a, b, 2021), respectively. For Mrk 573, Mrk 34, and Mrk 78, 1 arcsec corresponds to 349.1, 1007.7, and 747.4 pc in the galactic plane of each object, respectively (Revalski et al. 2021).

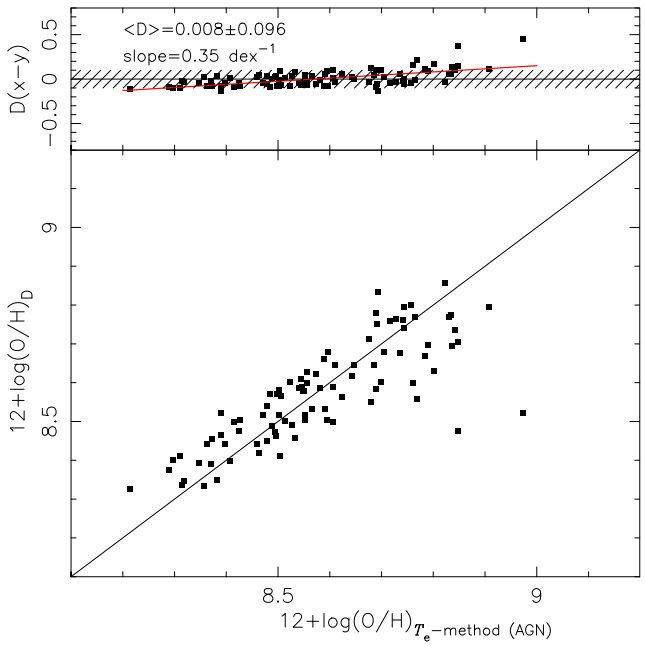

Figure 6. Bottom panel: Comparison between oxygen abundances [in units of 12 + log (O/H)] computed using the observational data described in Section 2.1 obtained through the D-method (y-axis, equation 9) and T_e-method (AGN) (x-axis; see Section 2.2). Solid line represents the equality between the estimates. Top panel: Difference ($D = x - y$) between the estimations versus those via T_e-method. The dashed area indicates the uncertainty of ±0.1 assumed in the oxygen abundance estimations (e.g. Denicoló, Terlevich & Terlevich 2002), while red line represents a linear regression to these differences whose slope is indicated. The average difference (<D>) is indicated.

Moran (2020), although it has been classified by them as semi-empirical calibration, is the first AGN calibration that takes into account O/H as reference values derived through the T_e-method instead of photoionization models.

In this work, we proposed an empirical calibration for AGNs between R_{23} and P line ratios with the O/H abundance, which is represented by a simple bi-dimensional expression (equation 9). In what follows, this approach (D-method) is a somewhat thorough discussion of its implications relative to other known methods in AGN studies. First of all, there are some concerns on the abundance determinations in AGNs via T_e-method. For instance, Stasińska (1984) compared observational emission-line ratio intensities of a sample of Seyfert 2 AGNs with those predicted by photoionization models. This author argued that the [O III](λ4959 + λ5003)/λ4363 ratio is enhanced by gas emission with very high electron density that precludes any abundance estimations in AGNs via the T_e-method (see also Nagao, Murayama & Taniguchi 2001). In fact, direct estimates of O/H abundance based on the same methodology of the T_e-method for SFs applied to AGN studies produce unreal low (subsolar) O/H values (see fig. 6 of Paper I) for most part of objects. However, these low values are not due to electron density effects but as a consequence of inappropriate use of the relations between temperatures of the low- and high-ionization gas zones derived for SFs in AGN chemical abundance studies (see Dors et al. 2020b; Riffel et al. 2021). Therefore, our O/H estimates following the adaptation of the T_e-method for AGNs by Dors et al. (2020b), in principle, are correct and can be used to derive empirical calibrations based on strong emission lines of AGNs. In fact, by inspecting Fig. 3 carefully, it can be seen that most parts of the sample present O/H abundance values close to or over the solar abundance [$12 + \log(\text{O/H})_\odot = 8.69$; Allende Prieto, Lambert & Asplund 2002] and few objects present equally subsolar O/H values (see also Groves, Heckman & Kauffmann 2006).

Another concern in that the value of an abundance indicator must not differ substantially across the area of the object type for which it will be considered in the estimation of abundances. Otherwise, the value of the abundance indicator measured from integrated flux might not be representative of the entire object. For SFs, Oey et al. (2000) found no spatial variation of the R_{23} across H II regions with distinct morphology (see also Oey & Shields 2000; Pilyugin 2001; Relaño et al. 2010; Mao, Lin & Kong 2018). In order to verify this in our case, the logarithm of R_{23} as a function of the distance (in arcsec) from the centre of three AGN nuclei Mrk 573, Mrk 34, and Mrk 78, whose data were taken from Revalski et al. (2018a, b, 2021), respectively, is shown in Fig. 5. Although a small decreasing of R_{23} is noted at external region (at distances larger than 2 arcsec or ∼1.5 kpc) from the centre of Mrk 78, we notice that R_{23} is relatively constant within the three objects. Therefore, similar to H II regions, R_{23} is a robust oxygen abundance indicator for AGNs.

In Fig. 6, bottom panel, a comparison between oxygen abundances [in units of 12 + log (O/H)] derived by using the D-method (equation 9) with estimations from the T_e-method (AGN) is performed. In Fig. 6, top panel, the difference (D) between these two methods versus the T_e-method (AGN) estimates is shown. There is a good agreement between the estimates for a wide range of O/H abundances, with D being approximately 0. However, we notice that the D-method (over) underestimates the O/H for the very (low) high metallicity regimes. In spite of the above observations, more objects with low and high metallicities are necessary to obtain a better conclusion. A comparison between O/H estimates derived assuming

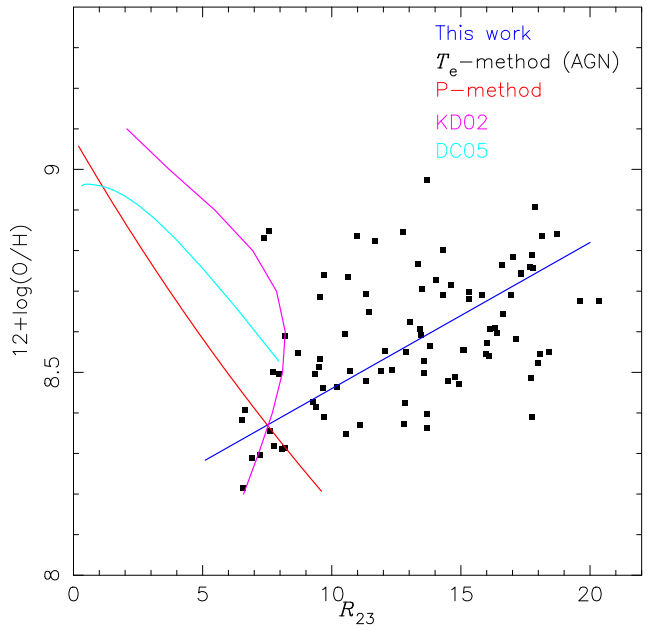

Figure 7. Oxygen abundances [in units of $12 + \log(\mathrm{O/H})$] versus R_{23}. Red, cyan, and pink lines represent SF calibrations proposed by Pilyugin (2001) (P-method, equation 10), Dors & Copetti (2005) (DC05), and Kewley & Dopita (2002) (KD02), respectively, as indicated. Blue line represents our calibration (equation 9). Points represent estimates via T_e-method (AGN) for our sample. Our calibration and the one by Pilyugin (2001) are shown for $P = 0.7$.

a vast number of methods available in the literature is presented in Paper I and it is repeated here.

Finally, we proceed with a comparison between our AGN O/H calibration and that of SFs. Particularly, this comparison can provide important pieces of information on the SED and physical processes in the gas phase of AGNs, and how they differ from those in SFs. In the light of the foregoing, the O/H–R_{23}, P relation for AGNs (equation 9), and the empirical calibration

$$12 + \log(\mathrm{O/H})_{\mathrm{P}} = \frac{R_{23}+54.2 + 59.45P + 7.31P^2}{6.07 + 6.71P + 0.371P^2+0.243R_{23}} \qquad (10)$$

for O/H determinations in SFs with moderately high metallicity [$12 + \log(\mathrm{O/H}) \gtrsim 8.2$] proposed by Pilyugin (2001) are shown in Fig. 7. In both calibrations, a fixed value of $P = 0.70$ is assumed, which is the mean value for our sample of AGNs. Also in Fig. 7, the R_{23} and O/H values derived via T_e-method (AGN) for our sample of objects, the semi-empirical calibration derived by Dors & Copetti (2005), and the theoretical calibration (assuming the ionizing parameter $q = 4 \times 10^7$ cm s^{-1}) proposed by Kewley & Dopita (2002) are shown. This q value represents an average value from the range of values considered by Kewley & Dopita (2002). It can be seen from Fig. 7 that our calibration and the T_e-method (AGN) estimates have a different behaviour between O/H and R_{23} relative to the calibrations for SFs, in the sense that R_{23} increases with the increase in O/H. In SFs, for the metallicity regime considered in Fig. 7, the decrease in R_{23} with the increase in O/H is mainly due to the decrease in the electron temperature and electrons with enough energy to excite the levels involved in producing the optical collisional excitation lines, in the case, R_{23}. Moreover, as increase in the metallicity occurs, effects of line blanketing by metal lines in the atmosphere of the ionizing star(s) become more pronounced (e.g. Zastrow, Oey & Pellegrini 2013), resulting in softer SED in stars and, consequently, decreasing R_{23}. A decrease in the ionization parameters (U) with the increase of metallicity (or O/H) can also contribute to a decrease in R_{23}. However, the dependence relations between these parameters are controversial in the literature (see Zinchenko et al. 2019, and references therein).

For AGNs, probably, SEDs are not affected by line blanketing or the NLRs are not significantly modified by changes in the SED, producing a direct relation between O/H and R_{23}. Ludwig et al. (2012) presented spectroscopic observations of 27 AGNs with some of the lowest black hole (BH) masses known and compared the emission-line ratios and SEDs of these objects with those of AGNs with higher mass BHs. These authors found evidence for steeper far-UV spectral slopes in lower mass systems in comparison with higher mass BHs. However, Ludwig et al. (2012) found similar NLR emission lines in objects with distinct BH masses. Also, Stern & Laor (2013) showed that parameters other than the ionizing continuum slope, such as metallicity, density, and ionization parameter, dominate the scatter in the BPT diagrams. Regarding the U-O/H dependence for AGNs, Pérez-Montero et al. (2019), based on Bayesian comparison between optical emission-line intensity ratios of a sample of AGNs and photoionization model results, found no correlation between these parameters. However, the sample considered by these authors consists of few objects (47 Seyfert 2); therefore, additional analysis is necessary to confirm this result.

5 CONCLUSIONS

The oxygen abundance estimates based on strong emission lines of Seyfert nuclei were investigated. Starting from the idea that the [O II]λλ3726, 3729 and [O III]λ5007 emission lines contain the necessary information to estimate the oxygen abundance in Seyfert nuclei and the T_e-method, adapted for AGNs, yields reliable abundance values, an empirical abundance calibration among R_{23}, P, and O/H was derived for AGNs. This calibration has been derived by using intensities of emission-line ratios from a sample of Seyfert 1 and 2 nuclei, whose data were taken from the SDSS DR7 and the line measurements carried out by the MPA/JHU group. No variation of R_{23} is observed inside AGNs, showing that this line ratio is a good O/H abundance indicator. The derived O/H $= f(R_{23}, P)$ relation produces, for a wide range of metallicities [$8.0 < 12 + \log(\mathrm{O/H}) < 9.2$], oxygen abundance values similar to those estimated via the T_e-method (AGN). In contrast to star-forming regions, the R_{23} line ratio increases with the increase of O/H in AGNs, indicating that the hardness of ionizing radiation is not affected by the metallicities in these kinds of objects or NLRs are not significantly modified by changes in the SED due to metallicity variations.

ACKNOWLEDGEMENTS

OLD is grateful to Fundacão de Amparo à Pesquisa do Estado de São Paulo (FAPESP) and Conselho Nacional de Desenvolvimento Científico e Tecnológico (CNPq).

DATA AVAILABILITY

The data underlying this article will be shared on reasonable request to the corresponding author.

REFERENCES

Abazajian K. N. et al., 2009, ApJS, 182, 543
Allende Prieto C., Lambert D. L., Asplund M., 2002, ApJ, 573, L137
Alloin D., Collin-Souffrin S., Joly M., Vigroux L., 1979, A&A, 78, 200
Antonucci R., 1993, ARA&A, 31, 473
Arellano-Córdova K. Z., Rodríguez M., 2020, MNRAS, 497, 672
Baldwin J. A., Phillips M. M., Terlevich R., 1981, PASP, 93, 5
Berg D. A., Skillman E. D., Croxall K. V., Pogge R. W., Moustakas J., Johnson-Groh M., 2015, ApJ, 806, 16
Bian F., Kewley L. J., Dopita M. A., 2018, ApJ, 859, 175
Blanton M. R. et al., 2017, AJ, 154, 28
Brown J. S., Martini P., Andrews B. H., 2016, MNRAS, 458, 1529
Campbell A., Terlevich R., Melnick J., 1986, MNRAS, 223, 811
Carvalho S. P. et al., 2020, MNRAS, 492, 5675
Castro C. S., Dors O. L., Cardaci M. V., Hägele G. F., 2017, MNRAS, 467, 1507
Contini M., 2017, MNRAS, 469, 3125
Croxall K. V., Pogge R. W., Berg D. A., Skillman E. D., Moustakas J., 2016, ApJ, 830, 4
De Robertis M. M., Dufour R. J., Hunt R. W., 1987, JRASC, 81, 195
Deharveng L., Peña M., Caplan J., Costero R., 2000, MNRAS, 311, 329
Denicoló G., Terlevich R., Terlevich E., 2002, MNRAS, 330, 69
Díaz Á. I., Terlevich E., Castellanos M., Hägele G. F., 2007, MNRAS, 382, 251
Dors O. L. J., Copetti M. V. F., 2003, A&A, 404, 969
Dors O. L. J., Copetti M. V. F., 2005, A&A, 437, 837
Dors O. L. J., Storchi-Bergmann T., Riffel R. A., Schimdt A. A., 2008, A&A, 482, 59
Dors O. L., Cardaci M. V., Hägele G. F., Krabbe Â. C., 2014, MNRAS, 443, 1291
Dors O. L., Cardaci M. V., Hägele G. F., Rodrigues I., Grebel E. K., Pilyugin L. S., Freitas-Lemes P., Krabbe A. C., 2015, MNRAS, 453, 4102
Dors O. L., Hägele G. F., Cardaci M. V., Krabbe A. C., 2017a, MNRAS, 466, 726
Dors O. L. J., Arellano-Córdova K. Z., Cardaci M. V., Hägele G. F., 2017b, MNRAS, 468, L113
Dors O. L. et al., 2020a, MNRAS, 492, 468
Dors O. L., Maiolino R., Cardaci M. V., Hägele G. F., Krabbe A. C., Pérez-Montero E., Armah M., 2020b, MNRAS, 496, 3209
Dors O. L., Contini M., Riffel R. A., Pérez-Montero E., Krabbe A. C., Cardaci M. V., Hägele G. F., 2021, MNRAS, 501, 1370
Edmunds M. G., Pagel B. E. J., 1984, MNRAS, 211, 507
Esteban C., Bresolin F., Peimbert M., García-Rojas J., Peimbert A., Mesa-Delgado A., 2009, ApJ, 700, 654
Feltre A., Charlot S., Gutkin J., 2016, MNRAS, 456, 3354
Flury S. R., Moran E. C., 2020, MNRAS, 496, 2191
Garnett D. R., 1992, AJ, 103, 1330
Gburek T. et al., 2019, ApJ, 887, 168
Groves B. A., Heckman T. M., Kauffmann G., 2006, MNRAS, 371, 1559
Hägele G. F., Díaz Á. I., Terlevich E., Terlevich R., Pérez-Montero E., Cardaci M. V., 2008, MNRAS, 383, 209
Hamann F., Korista K. T., Ferland G. J., Warner C., Baldwin J., 2002, ApJ, 564, 592
Izotov Y. I., Thuan T. X., 2008, ApJ, 687, 133
Izotov Y. I., Thuan T. X., Lipovetsky V. A., 1997, ApJS, 108, 1
Izotov Y. I., Stasińska G., Meynet G., Guseva N. G., Thuan T. X., 2006, A&A, 448, 955
Jensen E. B., Strom K. M., Strom S. E., 1976, ApJ, 209, 748
Jiang T., Malhotra S., Rhoads J. E., Yang H., 2019, ApJ, 872, 145
Jones T., Martin C., Cooper M. C., 2015, ApJ, 813, 126
Kennicutt Robert C. J., Bresolin F., Garnett D. R., 2003, ApJ, 591, 801
Kewley L. J., Dopita M. A., 2002, ApJS, 142, 35
Kewley L. J., Dopita M. A., Sutherland R. S., Heisler C. A., Trevena J., 2001, ApJ, 556, 121
Kewley L. J., Groves B., Kauffmann G., Heckman T., 2006, MNRAS, 372, 961
Kewley L. J., Nicholls D. C., Sutherland R. S., 2019, ARA&A, 57, 511
Krabbe A. C., Oliveira C. B., Zinchenko I. A., Hernández-Jiménez J. A., Dors O. L., Hägele G. F., Cardaci M. V., Telles N. R., 2021, MNRAS, 505, 2087
Kraemer S. B., Wu C.-C., Crenshaw D. M., Harrington J. P., 1994, ApJ, 435, 171
Liang Y. C., Hammer F., Yin S. Y., Flores H., Rodrigues M., Yang Y. B., 2007, A&A, 473, 411
Lopez-Sanchez A. R., Esteban C., 2010, preprint (arXiv:1004.5251)
Ludwig R. R., Greene J. E., Barth A. J., Ho L. C., 2012, ApJ, 756, 51
McGaugh S. S., 1991, ApJ, 380, 140
Maiolino R., Mannucci F., 2019, A&AR, 27, 3
Mao Y.-W., Lin L., Kong X., 2018, ApJ, 853, 151
Marino R. A. et al., 2013, A&A, 559, A114
Mignoli M. et al., 2019, A&A, 626, A9
Morales-Luis A. B., Pérez-Montero E., Sánchez Almeida J., Muñoz-Tuñón C., 2014, ApJ, 797, 81
Nagao T., Murayama T., Taniguchi Y., 2001, ApJ, 549, 155
Netzer H., Ferland G. J., 1984, PASP, 96, 593
Oey M. S., Shields J. C., 2000, ApJ, 539, 687
Oey M. S., Dopita M. A., Shields J. C., Smith R. C., 2000, ApJS, 128, 511
Osterbrock D. E., Miller J. S., 1975, ApJ, 197, 535
Pagel B. E. J., Edmunds M. G., Blackwell D. E., Chun M. S., Smith G., 1979, MNRAS, 189, 95
Pagel B. E. J., Simonson E. A., Terlevich R. J., Edmunds M. G., 1992, MNRAS, 255, 325
Peimbert M., Peimbert A., Delgado-Inglada G., 2017, PASP, 129, 082001
Pérez-Montero E., 2014, MNRAS, 441, 2663
Pérez-Montero E., 2017, PASP, 129, 043001
Pérez-Montero E., Contini T., 2009, MNRAS, 398, 949
Pérez-Montero E., Dors O. L., Vílchez J. M., García-Benito R., Cardaci M. V., Hägele G. F., 2019, MNRAS, 489, 2652
Pettini M., Pagel B. E. J., 2004, MNRAS, 348, L59
Pilyugin L. S., 2000, A&A, 362, 325
Pilyugin L. S., 2001, A&A, 369, 594
Pilyugin L. S., 2003, A&A, 399, 1003
Pilyugin L. S., 2007, MNRAS, 375, 685
Pilyugin L. S., Grebel E. K., 2016, MNRAS, 457, 3678
Pilyugin L. S., Vílchez J. M., Thuan T. X., 2006, MNRAS, 370, 1928
Pilyugin L. S., Grebel E. K., Mattsson L., 2012, MNRAS, 424, 2316
Relaño M., Monreal-Ibero A., Vílchez J. M., Kennicutt R. C., 2010, MNRAS, 402, 1635
Revalski M., Crenshaw D. M., Kraemer S. B., Fischer T. C., Schmitt H. R., Machuca C., 2018a, ApJ, 856, 46
Revalski M. et al., 2018b, ApJ, 867, 88
Revalski M. et al., 2021, ApJ, 910, 139
Riffel R. A. et al., 2021, MNRAS, 501, L54
Sanders R. L. et al., 2016, ApJ, 825, L23
Sarazin C. L., 1976, ApJ, 208, 323
Schmitt H. R., 1998, ApJ, 506, 647
Searle L., 1971, ApJ, 168, 327
Shaver P. A., McGee R. X., Newton L. M., Danks A. C., Pottasch S. R., 1983, MNRAS, 204, 53
Shaw R. A., Dufour R. J., 1995, PASP, 107, 896
Shi F., Zhao G., Liang Y. C., 2007, A&A, 475, 409
Shields G. A., Searle L., 1978, ApJ, 222, 821
Stasińska G., 1978, A&AS, 32, 429
Stasińska G., 1984, A&A, 135, 341
Stasińska G., Collin-Souffrin S., Joly M., Alloin D., 1981, A&A, 93, 362
Stern J., Laor A., 2013, MNRAS, 431, 836
Storchi-Bergmann T., Calzetti D., Kinney A. L., 1994, ApJ, 429, 572
Storchi-Bergmann T., Schmitt H. R., Calzetti D., Kinney A. L., 1998, AJ, 115, 909
Thomas A. D., Dopita M. A., Kewley L. J., Groves B. A., Sutherland R. S., Hopkins A. M., Blanc G. A., 2018, ApJ, 856, 89
Tody D., 1986, in Crawford D. L., ed., Proc. SPIE Conf. Ser. Vol. 627, Instrumentation in Astronomy VI. SPIE, Bellingham, p. 733

Toribio San Cipriano L., Domínguez-Guzmán G., Esteban C., García-Rojas J., Mesa-Delgado A., Bresolin F., Rodríguez M., Simón-Díaz S., 2017, MNRAS, 467, 3759
Torres-Peimbert S., Peimbert M., 1977, Rev. Mex. Astron. Astrofis., 2, 181
van Zee L., Salzer J. J., Haynes M. P., O'Donoghue A. A., Balonek T. J., 1998, AJ, 116, 2805
Vaona L., Ciroi S., Di Mille F., Cracco V., La Mura G., Rafanelli P., 2012, MNRAS, 427, 1266
Viegas S. M., 2002, in Henney W. J., Franco J., Martos M., eds, Rev. Mex. Astron. Astrofis. Ser. Conf. Vol. 12, Ionized Gaseous Nebulae. UNAM, Mexico City, p. 219
Yates R. M., Schady P., Chen T. W., Schweyer T., Wiseman P., 2020, A&A, 634, A107
Yin S. Y., Liang Y. C., Hammer F., Brinchmann J., Zhang B., Deng L. C., Flores H., 2007, A&A, 462, 535
York D. G. et al. 2000, AJ, 120, 1579
Zastrow J., Oey M. S., Pellegrini E. W., 2013, ApJ, 769, 94
Zhang K., Wang T., Dong X., Lu H., 2008, ApJ, 685, L109
Zinchenko I. A., Dors O. L., Hägele G. F., Cardaci M. V., Krabbe A. C., 2019, MNRAS, 483, 1901

This paper has been typeset from a TEX/LATEX file prepared by the author.